

TARGET detection is the process of bringing a salient stimulus into conscious awareness. Target detection evokes a prominent event-related potential (ERP) component (P3) in the electroencephalogram (EEG). We combined the high spatial resolution of functional magnetic resonance imaging (fMRI) with the high temporal resolution of EEG to investigate the neural generators of the P3. Event-related brain activation (ERBA) and ERPs were computed by time-locked averaging of fMRI and EEG, respectively, recorded using the same paradigm in the same subjects. Target detection elicited significantly greater ERBAs bilaterally in the temporal–parietal cortex, thalamus and anterior cingulate. Spatio-temporal modelling of ERPs based on dipole locations derived from the ERBAs indicated that bilateral sources in the temporal–parietal cortex are the main generators of the P3. The findings provide convergent fMRI and EEG evidence for significant activation of the temporal–parietal cortex 285–610 ms after stimulus onset during target detection. The methods developed here provide a novel multimodal neuroimaging technique to investigate the spatio-temporal aspects of processes underlying brain function.

Key words: Dipoles; ERP; Event-related; fMRI; P3; Single trial

Combined event-related fMRI and EEG evidence for temporal–parietal cortex activation during target detection

V. Menon,^{1,3,CA} J. M. Ford,^{1,3}
K. O. Lim,^{1,3} G. H. Glover²
and A. Pfefferbaum^{1,4}

Departments of ¹Psychiatry and Behavioral Sciences, MC 5548 and ²Radiology, Stanford University School of Medicine, Stanford, CA 94305; ³Palo Alto VA Health Care System, and ⁴SRI International, USA

CA,¹Corresponding Author and Address

Introduction

Monitoring the environment for change and deciding on a course of action when changes are detected are critical operations for survival. It involves many component processes which can be studied in the laboratory setting by the use of simplified detection paradigms. In one such, the ‘oddball’ paradigm, subjects detect and respond to infrequent (oddball) target events embedded in a series of repetitive events.¹ Following initial sensory processing, target detection involves the process of bringing a salient stimulus into conscious awareness for further evaluation, categorization and response.² This process elicits a distinct bio-electric response in the brain that can be detected in the electroencephalogram (EEG). Stimulus synchronized averaging of EEG response yields an event-related brain potential (ERP) that provides the millisecond temporal resolution needed to investigate the timing of brain processes. Target detection elicits a large positive component, 300 ms and 600 ms after stimulus onset, which is maximal over the parietal scalp: the parietal P3 or P3b. The P3b is thought to reflect directed, effortful processing underlying target detection.³

The P3b is relatively unaffected by the physical attributes of the stimuli; it is a brain signal that marks the completion of initial sensory processing and the onset of a process of directed attention leading to conscious awareness of salient stimuli. The P3b is preceded by a small positive component over the frontal lobe, P3a, that peaks between 250 ms and 500 ms and is thought to reflect an initial automatic orienting response.³ During the past three decades the P3a and P3b have been widely used to study brain responses to novelty, uncertainty, attention, memory, affect and biological state.⁴ They have also been used widely to investigate cognitive dysfunction that accompanies many psychiatric diseases and aging.^{4,5}

The specific brain areas involved in target detection and their relation to scalp recorded P3 potentials in neurologically normal humans is largely unknown. It is mathematically impossible to determine neural sources from the scalp recorded ERPs. A number of current distributions in the brain can give rise to identical field distributions on the scalp⁶. Thus other approaches are needed to determine ERP component genesis. Intracranial recordings in patients undergoing neurosurgery and scalp

recordings in patients with brain lesions have suggested multiple distributed P3 generators in the thalamus, inferior parietal lobe, hippocampus, superior temporal gyrus, dorsolateral prefrontal cortex, anterior cingulate and orbito-frontal cortex.⁷⁻¹¹ However, the differential contributions of these brain regions to target detection is unclear. Positron emission tomographic (PET) studies have identified the anterior cingulate as involved in target detection and selection,¹² but it is not clear whether the activation is due to increased task demands (e.g. increased attention) or to any specific aspects of target detection and response selection.

In this study we combined the superior spatial resolution of fMRI with the superior temporal resolution of ERPs to study the spatio-temporal characteristics of brain activation during the oddball task in neurologically normal subjects. Unlike earlier PET and fMRI studies, which compared brain responses to blocks of task and control stimulus sequences, we presented both stimulus types in a single 'oddball' sequence and designed analysis methods to determine event-related brain activation (ERBA) from fMRI signals in a manner analogous to the determination of ERPs from EEG signals. We used an interstimulus interval (ISI) of 8 s, rather than the typical 1-2 s used in oddball ERP paradigms, to avoid any overlap in the hemodynamic responses between consecutive infrequent targets. The mean time interval between consecutive infrequent target events was 40 s, long enough to ensure complete recovery of the hemodynamic response to baseline levels.¹³ This enabled determination of brain areas that showed time-locked activation to infrequent target events.

Three analyses were performed. First, ERBAs were derived from fMRI time series, then ERPs were derived from the EEGs and, finally, dipole sources derived from ERBA foci were used to model the time course of the ERP scalp distribution.

Materials and Methods

Subjects: Eleven healthy right-handed subjects (five men and six women; aged 20-35 years; mean 24 years) participated in the study after giving written informed consent. Each subject performed the same task on two occasions, first with MR scanning and 2 weeks later with EEG recording.

Task: The stimulus sequence comprised eighty 1000 Hz (frequent) and twenty 2000 Hz (infrequent) tones of 150 ms duration presented randomly with an ISI of 8 s. Subjects were instructed to respond with a right hand index finger press immediately after hearing the infrequent tone.

fMRI: Images were acquired on a conventional 1.5T GE scanner using a quadrature whole head coil. Subjects lay supine in the scanner with their head restrained using a bitebar.¹⁴ Functional images were acquired using a T2* weighted gradient echo spiral pulse sequence with a temporal resolution of 2 s at 400 time points (TR = 67 ms, TE = 40 ms, flip angle = 40° and 4 interleaves).¹⁵ At each time point, six axial slices, 0-42 mm above the anterior commissure, were imaged. Slice thickness was 6 mm, interslice thickness 1 mm, field of view 310 mm, with an effective inplane spatial resolution of 4.35 mm. A single k-space image file was written to disk and images reconstructed, by inverse Fourier transform, for each of the 400 time points into 256 × 256 × 6 image matrices (resolution: 1.21 × 1.21 × 7 mm). Images corresponding to the first four time points were discarded from further analysis to eliminate non-equilibrium effects.

The task was programmed using Psyscope (<http://poppy.psy.cmu.edu/psyscope>) on a Macintosh notebook computer. Onset of scanning and task were synchronized using a TTL pulse delivered to the scanner timing microprocessor board from a 'CMU Button Box' microprocessor connected to the Macintosh with a serial cable. Audio signals from the Macintosh were amplified using a home audio receiver and transmitted to a piezo-electric speaker placed near the head of the scanner. Sound was piped binaurally to the subjects by means of a plastic headset connected with a plastic tube to a funnel placed over the piezo-electric speaker.

fMRI data were pre-processed using SPM96 (<http://www.fil.ion.ucl.ac.uk/spm>). Images were corrected for movement using least square minimization without higher-order corrections for spin history.¹⁶ Images were normalized to stereotaxic Talairach coordinates,¹⁷ resampled every 2 mm using sinc interpolation and spatially smoothed with a uniform three dimensional Gaussian filter with a full width at half maximum (FWHM) of 4 mm. The spiral gradient echo recalled fMRI images used in the present study have an effective in-plane spatial resolution of 4.35 mm and an out-of-plane resolution of 7 mm. The effect of spatial smoothing with a 4 mm FWHM kernel is therefore minimal and mainly ensured spatial homogeneity along all three spatial axes.

To determine brain regions that showed significantly greater time-locked activation to infrequent targets, regression analysis and the theory of Gaussian random fields as implemented in SPM96 was used. This analysis assumes that the underlying distribution statistics can be modeled by homogeneous and isotropic random fields with a Gaussian (spatial) autocorrelation. A discussion of the strengths and weaknesses of this approach is presented elsewhere.¹⁸ Time series regression analysis,

as opposed to straightforward time-locked averaging, was used to take advantage of the statistical power of the general linear model, and to take into account corrections for temporal and spatial autocorrelations in the fMRI data.^{19–21} Multisubject averaging was used to enhance signal detection power, with a regression analysis blocked design matrix that ensured a very large number of degrees of freedom. The statistical parametric maps thus derived represent ERBAs to infrequent targets.

Voxel-wise *t*-statistics were computed using multivariate linear regression. A predictor reference waveform (1 for images corresponding to the infrequent tone and 0 for all other images), convolved with the haemodynamic response function (HRF), was used to determine activation directly related to infrequent tones. The HRF was a Poisson function with a delay of 6 s.^{13,22} The confounding effects of fluctuations in global mean were removed with an ANCOVA model. Low frequency noise was removed with a high pass filter (0.5 cycles/min) applied to the fMRI time series at each voxel. A temporal smoothing function (Gaussian kernel corresponding to dispersion of 8 s) was applied to the fMRI time series to enhance the signal to noise ratio. The degrees of freedom were adjusted to take into account autocorrelations in the fMRI time series. The *t*-statistics were normalized to *Z* scores. Cluster-level significance levels were derived based on the joint distribution of height and extent of *Z* scores. A significance level threshold of $Z > 3.09$ (corresponding to $p < 0.001$, corrected for multiple spatial comparisons) was used to determine the presence of significant activation foci. The number of degrees of freedom in the regression analysis was 1100. The volume analyzed was 49 705 voxels, 595 resolution elements. Smoothness along the three axes were 8.7, 7.8, and 9.8 mm. To be considered significant each cluster had to have at least 68 contiguous voxels with *Z* value > 3.09 .

MRI: High resolution whole brain images were acquired to assist localization of activation foci. These images were acquired using a T1 weighted spoiled grass gradient recalled (SPGR) 3D MRI sequence with the following parameters: TR = 24 ms; TE = 5 ms; flip angle = 40°; 24 cm field of view; 124 slices in sagittal plane; 256 × 192 matrix; acquired resolution = 1.5 × 0.9 × 1.2 mm. The reconstructed image was a 124 × 256 × 256 matrix (resolution: 1.5 × 0.9 × 0.9 mm).

EEG: EEGs were recorded from 19 standard 10–20 scalp sites using the Neuroscan EEG acquisition system (Neuroscan Inc., VA, USA) and electrogel electrodes (Physiometrix Inc., MA, USA) with a linked mastoid reference. Vertical and horizontal

oculograms (VEOG and HEOG) were recorded with bipolar electrodes. Recording gains were 10k for EEG and 3k for EOG channels. Data were acquired with a sampling rate of 200 Hz and band pass filtered at 0.1–30 Hz. Subjects sat comfortably in an electromagnetically shielded Faraday cage and were presented with auditory tones using the STIM stimulus presentation hardware and software (Neuroscan Inc.). Stimulus markers and EEG were saved on disk for further analysis.

Single trials at each electrode were individually corrected for the effects of eye movements. A 100 ms prestimulus baseline was removed from each trial and trials with voltages above or below $\pm 200 \mu\text{V}$ were rejected. ERPs to correctly identified infrequent tones and frequent tones were computed and difference waveforms were derived by subtracting the frequent from the infrequent ERPs.

P3 signals elicited with an 8 s ISI sequence were compared with that elicited with a more standard oddball sequence, with 1 s ISIs, from 10 young subjects (19–28 years old, mean 23 years; eight men). Peak ERP amplitudes in the interval 300–600 ms, from electrodes Fz, Cz and Pz, to frequent and infrequent stimuli, were analyzed using ANOVA with Geisser–Greenhouse corrections.

fMRI and EEG: The potential distribution on the scalp due to a dipole with specified location and orientation was computed using a three-shell spherical model consisting of concentric cortex, skull and scalp layers.²³ The scalp and cortex conductivities were 1 and the skull conductivity was 1/80. For each dipole, potentials were computed at 19 scalp sites in the 10–20 system and summed. Radii of the cortex, skull and scalp were derived from the averaged Talairach normalized MRIs. Mean radius of the cortical shell was estimated to be the mean of the radii in the three orthogonal directions. The radius of this sphere was 75 mm. The average skull and scalp thickness were estimated to be 6 mm and 5 mm respectively.

The translation and rotation needed to transform dipole locations from the Talairach coordinates to the 10–20 coordinate system were estimated based on previously published methods to determine 10–20 electrode locations from MRI landmarks.^{24–26} In Talairach coordinates, the center of the three-shell sphere described above was 15 mm posterior to the AC in the midsagittal plane along the AC–PC line (i.e., [0, –15, 0] mm in Talairach coordinates). The anterior–posterior direction of the 10–20 coordinate system was then defined along the line between this center and the Nasion which was identified on the average MRI. In the midsagittal plane, the angle between the anterior–posterior directions in the

10-20 and the Talairach coordinate systems was 16 degrees. These values of translation and rotation were used to transform dipole locations in Talairach coordinates to the 10-20 coordinate system and *vice versa*.

Dipole locations were kept fixed but the orientation was varied to determine the best-fitting dipole orientation that matched the scalp distribution of the maximum ERP difference. Best-fitting dipole orientations were determined by computing the correlation between the actual and model ERP distributions. Correlations were enumerated at all angles with an increment of 0.1°. This avoided potential problems of local minima that could affect non-linear optimization methods. Because of the symmetry, only three orientations needed to be varied. Correlation between the actual and computed distributions was used as the measure of goodness of fit. Finally, with the dipole location and orientations fixed, correlations between the ERP difference waveform and the dipole model distributions were determined over the period from 100 ms before to 1000 ms after stimulus onset.

Results

Subjects performed the task correctly, as judged by the 93% accuracy rate. Mean reaction time for correctly identified targets was 529 ms. Statistical parametric maps, representing ERBAs to infrequent targets, derived from multisubject averages revealed four significant clusters of activity, with primary peaks in the left and right supramarginal gyri (BA 40), left thalamus, and anterior cingulate (BA 24) and additional secondary peaks in the left supramarginal gyrus and right thalamus (Table 1). Fig. 1 shows the precise locations of these activations superimposed on averaged Talairach-normalized high resolution structural MRIs. The largest and most significant

Table 1. Brain areas that showed significantly greater activation to target stimuli based on average across 11 subjects

Area	Location			Z	No. voxels
L supramarginal gyrus (BA 40)	-60	-32	30	6.10	359
<i>L supramarginal gyrus (BA 40)</i>	<i>-56</i>	<i>-48</i>	<i>32</i>	<i>4.79</i>	
R supramarginal gyrus (BA 40)	62	-34	24	5.80	182
L thalamus	-12	-12	20	5.54	234
<i>R thalamus</i>	<i>4</i>	<i>-10</i>	<i>18</i>	<i>5.14</i>	
Anterior cingulate (BA 24)	2	-6	40	4.73	216

The Talairach coordinates, the Z scores and size of the activated area are shown. The locations and Z scores of statistically significant secondary maxima within these areas are shown in italic. The activations were significant at $p < 0.001$ ($Z > 3.09$) after correction for multiple spatial comparisons.

activations were in the left and right supramarginal gyri, adjacent to the posterior ascending ramus of the sylvian fissure (Fig. 2A). Activated thalamic regions correspond most closely with the anterior nucleus. The activated anterior cingulate area corresponds most closely with area 24a' and 24b' in the mid-cingulate gyrus.²⁷

In order to verify that the derived ERBA maps correspond directly to processing of infrequent targets, fMRI time series images were first averaged across subjects. Individual fMRI trials corresponding to infrequent tones were then averaged after removal of low frequency noise (high pass filter: 0.5 cycles/min). A prestimulus baseline of 4 s was removed. Signal increases of 0.3–0.6% above baseline were observed to infrequent target events in each of the regions that showed significant ERBA activation. Figure 2B shows the time locked signal changes in the left and right supramarginal gyri following onset of target events. The time course of the activation indicates a delay and dispersion of approximately 8 s. The analysis confirmed the validity of computing time-locked ERBAs to infrequent targets using time-series regression analysis.

ERPs to infrequent and frequent tones were averaged from individual EEG trials and difference waveforms computed. Infrequent tones elicited P3b, maximal at electrode Pz (midline parietal scalp), with peak latency at 350 ms in the multisubject grand average (Fig. 3A). This component was significantly larger to the infrequent than to the frequent tone ($t(10) = 5.96$, $p < 0.0001$). Difference waveforms were greatest at electrode Pz at 385 ms with amplitudes of 7.5, 6.4, and 6.6 mV at electrodes Pz, P3 and P4, respectively (Fig. 3B). Compared to the 1 s ISI sequence, the 8 s ISI sequence elicited larger P3b signals ($F(1,19) = 14.76$, $p < 0.005$). However, the difference between the P3bs to infrequent and frequent stimuli were not significantly different (ISI \times stimulus; $F(1,19) = 1.20$, n.s.). The scalp distribution of P3b was not different for the two ISIs (ISI \times electrode: $F(2,38) = 1.57$, n.s.), nor was there an interaction of these three variables (ISI \times stimulus \times electrode: $F(2,38) = 0.43$, n.s.). This confirmed the validity of using an 8 s ISI sequence to investigate the P3.

To compare electrophysiological and fMRI data, the scalp ERP distribution was modeled using dipole source locations derived from the ERBAs and a spherical three shell model. Two symmetrical dipole current sources were placed at the locations of maximal ERBAs determined from fMRI in the left and right supramarginal gyri (Fig. 1) and their potentials were summed at the 19 scalp electrode sites. In the 10-20 electrode system, the dipole sources were located close to the mid-point of electrodes C3, P3,

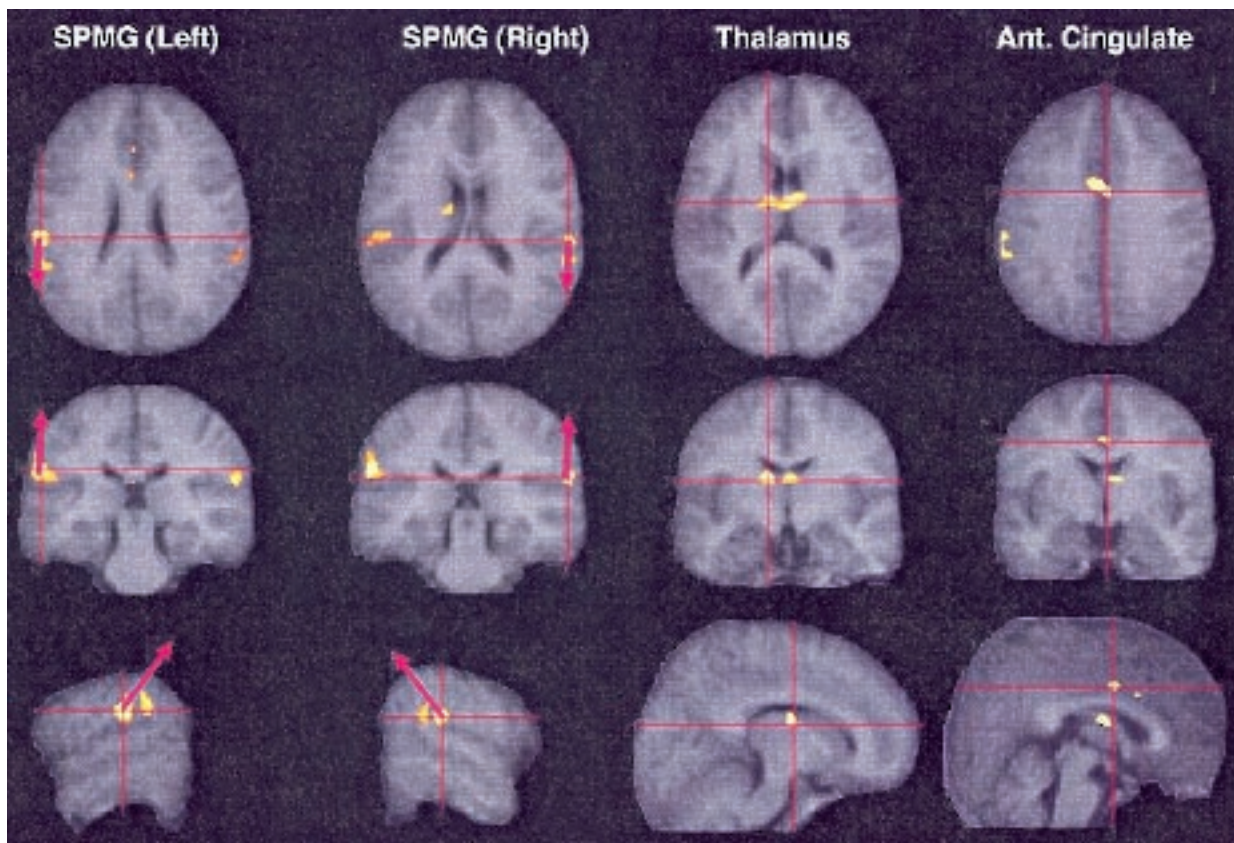


FIG. 1. Brain areas that showed significant fMRI activation to target stimuli are shown superposed on average MRI in Talairach space: left and right supramarginal gyri (SPMG), thalamus and anterior cingulate. Cross hairs mark locations of peak activation. Bilateral symmetric dipole sources (indicated by arrows) in the left and right supramarginal gyri are the main generators of the P3b component of ERP to infrequent target stimuli. Note that the dipole orientations are approximately perpendicular to the cortical gray matter. The dipole sources are active 285–610 ms following target stimulus onset. The length of the arrows indicate the relative strengths of the dipoles in the three orthogonal planes.

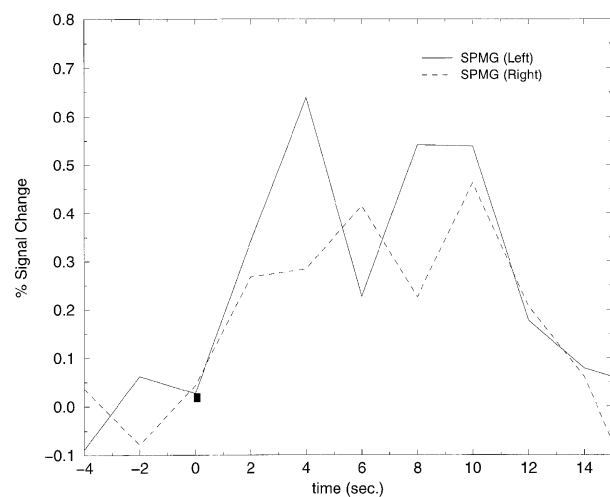
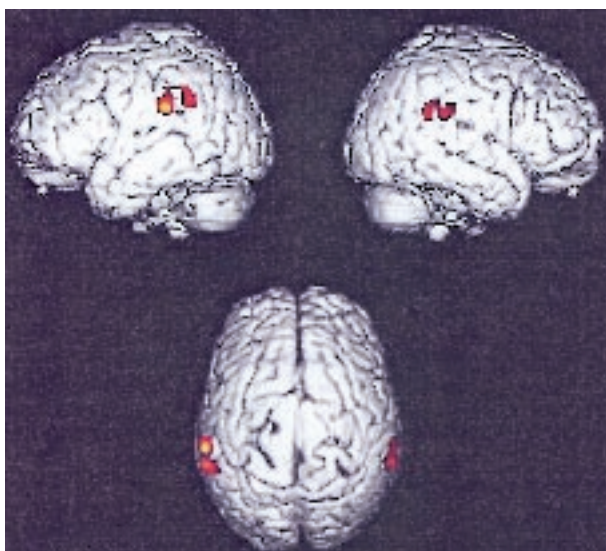


FIG. 2. (A) Surface rendered bilateral event related fMRI activation to target stimuli in the supramarginal gyri (Brodmann area 40) near the posterior ascending ramus of the sylvian fissure. Left and right hemisphere activations are roughly symmetric. Unilateral lesions of this region have been shown to abolish the P3b component of the ERP to infrequent targets. (B) Time-locked average of fMRI images to 20 infrequent target stimuli at locations of maximal left and right supramarginal gyrus activation. A prestimulus baseline of 4 s was removed.

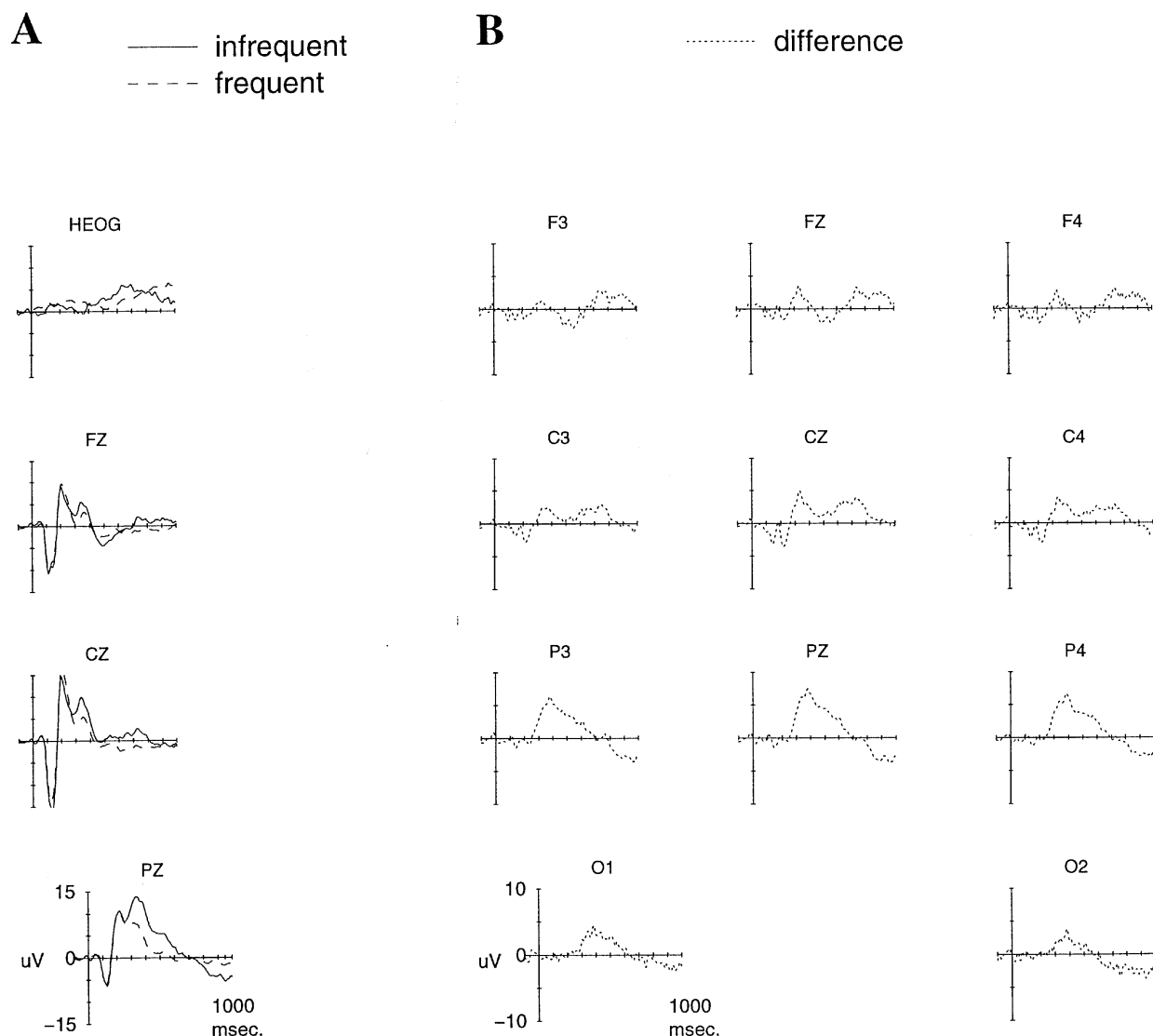
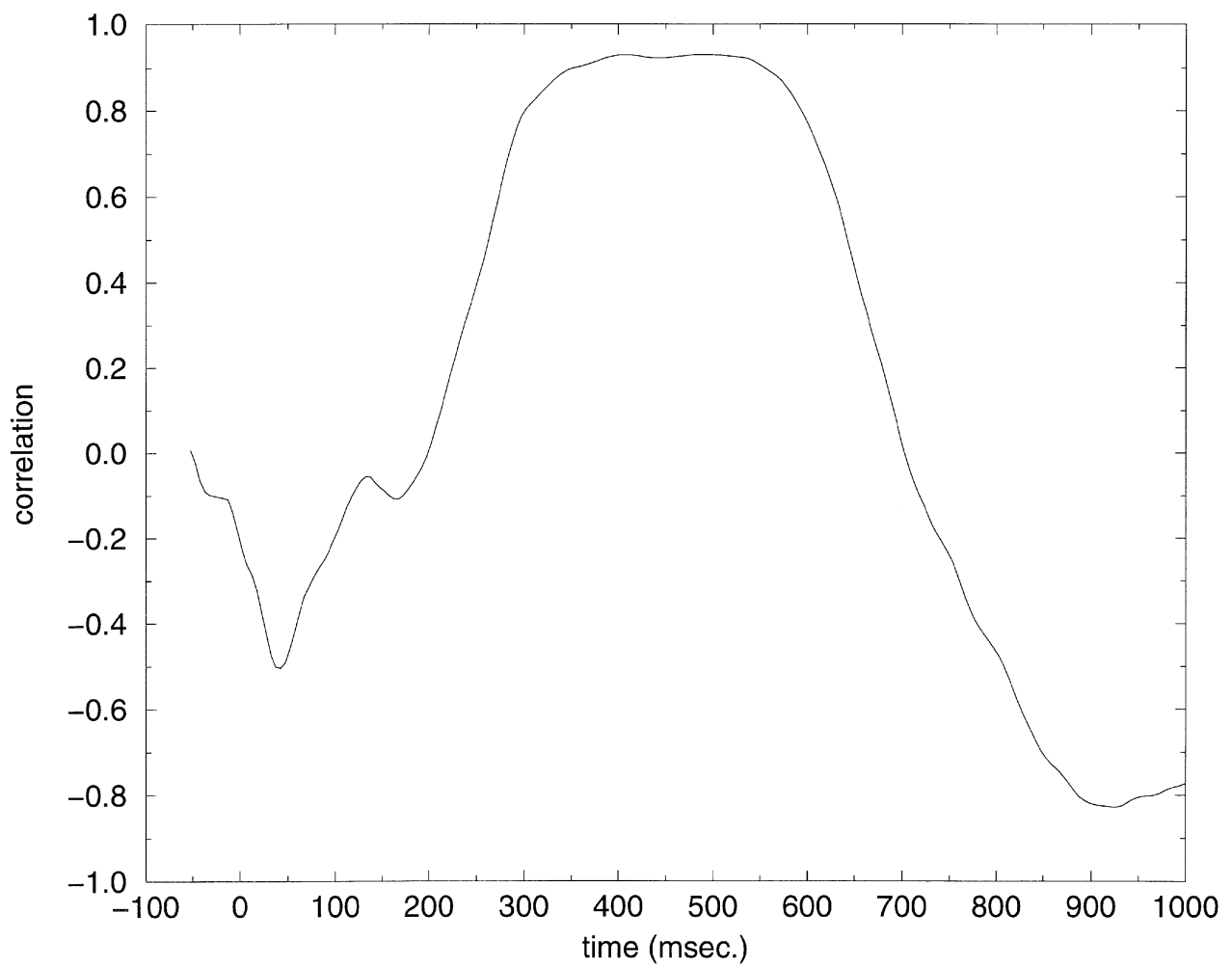
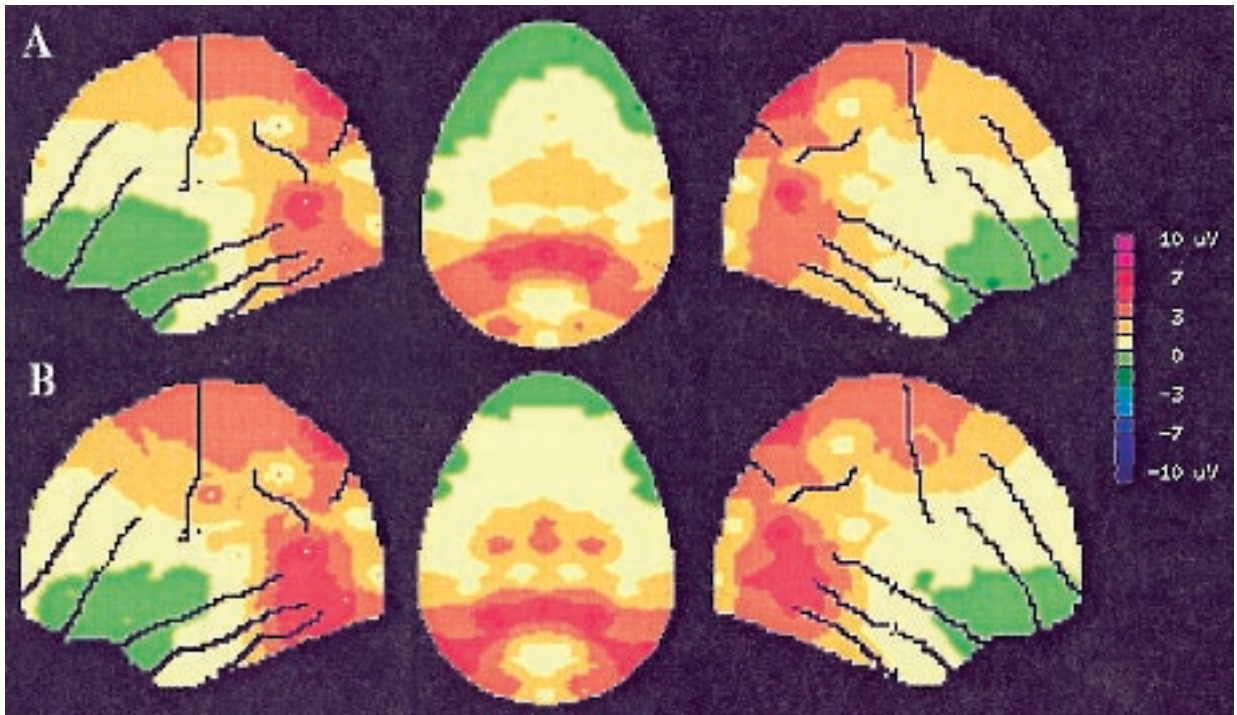


FIG. 3. (A) Time-locked event-related potentials (ERPs) to infrequent target and frequent stimuli recorded on midline electrodes Fz, Cz and Pz. The ERPs to the two stimuli are almost identical until about 200 ms, at which point a parietal P3b component to the infrequent target events is activated. (B) Difference of ERPs to infrequent target and frequent stimuli on a subset of the 19 scalp electrodes. The largest differences were recorded at electrodes Pz, P3 and P4: 7.5, 6.4 and 6.6 μV , respectively, 385 ms following stimulus onset. Grand average across 11 subjects.

T3 and T5 in the left hemisphere and C4, P4, T4 and T6 in the right hemisphere. The thalamus and anterior cingulate, though activated on ERBAs, were excluded from this model as they were not expected to contribute significantly to scalp recorded potentials. Thalamic nuclei do not have the layered organization of the cortex needed to generate far fields

that can be recorded on the scalp.²⁸ Dipole fields decrease as square of distance from source. The anterior cingulate activation is farther (45 mm) from the scalp surface than the supramarginal gyrus activation (approximately 17 mm) and thus contributes seven times less to the scalp potentials than the supramarginal gyrus.

FIG. 4. (A) Scalp distributions of the observed difference waveform ERP and (B) dipole source model derived from fMRI activation at 385 ms following target stimulus onset. Correlation between the two distributions was 0.95 ($p < 0.001$). The dipole sources are located close to the mid-point of electrodes C3, P3, T3 and T5 in the left hemisphere and C4, P4, T4 and T6 in the right hemisphere. The three columns show left, top and right views. (C) Correlation between the observed and dipole model scalp ERP distributions as a function of time after target onset. The two distributions were significantly correlated only in the interval 285–610 ms following stimulus onset. Dipole source locations and orientations were kept fixed.



With dipole source locations fixed in the supramarginal gyrus, the orientation was varied to determine the best-fitting dipole orientation that matched the scalp distribution of the ERP difference waveform at 385 ms. The computed best-fit potential distributions were highly correlated with observed ERP distributions (correlation coefficient, 0.95, $p < 0.001$, $F(1,17) = 15.7$) and had a similar scalp topography (Fig. 4A). Both the distributions have maxima at Pz, large amplitudes at P3 and P4, and are approximately symmetrical across hemispheres. The best-fitting dipole orientation was transformed back from the 10-20 coordinate system to Talairach space and superposed on the average MRI (Fig. 1). The dipole is oriented 1° to the anterior-posterior axis in the axial plane, 0.7° to the inferior-superior axis in the coronal plane, and 37° to the inferior-superior axis in the sagittal plane. In the axial and coronal planes these orientations can be clearly identified as being perpendicular to cortical gray matter, in agreement with electrophysiological and anatomical constraints.²⁹

Finally, with the dipole location and orientations fixed, correlations between the ERP difference waveform and the dipole model distributions were determined over a period from 100 ms before to 1000 ms after stimulus onset. Between 285 ms and 610 ms correlations exceeded 0.7 ($p < 0.001$, $F(1,17) = 15.7$; Fig. 4B) but they were not significant at any other time outside this latency window.

Discussion

The analysis suggests that (1) the dominant contribution to the scalp P3b arises from bilateral activation of superficial sources in the supramarginal gyrus and (2) these generators are activated in the interval 285–610 ms following target stimulus onset. The results are in excellent agreement with studies showing that unilateral lesions to the temporal-parietal cortex abolish the scalp P3b.¹¹ Large intracranial P3 signals have been recorded in and around this region.^{8,9} These findings provide convergent fMRI and EEG evidence for significant activation of the supramarginal gyrus during target detection. The results suggest that the supramarginal gyrus is critically involved in generating a prominent brain signal involved in post-sensory processing of salient stimuli for evaluation, categorization, response and decision making. This region in the temporal-parietal cortex is ideally suited for such a role since it receives extensively pre-processed information from multiple sensory-specific and heteromodal association areas.³⁰

In addition to the supramarginal gyrus, the anterior cingulate and the thalamus appear to be critically involved in target detection. These ERBA sites are

also consistent with intracranial recordings indicating the presence of large electrical potentials to target stimuli in the P3 latency range.^{7,10} Besides being a key component in the anterior vigilance attention network, the anterior cingulate may be directly involved in target detection and response selection. The area of the brain activated in the anterior cingulate gyrus corresponds most closely to caudal area 24' in the cognitive and executive region of the anterior cingulate. Several studies have previously indirectly implicated this brain region in response selection.³¹ The smaller and deeper activation of the anterior cingulate may underly the smaller fronto-central component of the scalp P3 (P3a) which characterizes the initial orienting response preceding P3b. These observations suggest that direct projections from the anterior cingulate may initiate or modulate activation of the supramarginal gyrus.

The thalamic activation in the present study, localized primarily to the anterior nucleus, is consistent with the notion of a hippocampal-hypothalamic network mediating the initial orienting response.^{3,32} The anterior nucleus is the relay for the limbic system; it receives input from the hippocampus via afferents from the hypothalamus and sends efferents to the cingulate gyrus. The possible participation of the hippocampus in target detection remains to be investigated.

Conclusion

Our results, together with other recent studies, demonstrate that brain responses to individual stimulus types and events can be investigated using functional MRI.^{33–36} This provides a more direct way of probing mental activity than standard fMRI and PET paradigms where task conditions with mixed events are compared. More broadly, the present method permits combining the high spatial resolution of fMRI with the high temporal resolution of ERPs in a single paradigm. This will significantly enhance our ability to investigate an important aspect of brain function: the timing of neuronal events in distributed networks.

References

1. Sutton S, Braren M, Zubin J et al. *Science* **150**, 1187–1188 (1965).
2. Posner MI and Raichle ME. *Images of Mind*. New York: WH Freeman, 1994: 168–1712.
3. Knight RT. *Nature* **383**, 256–259 (1996).
4. Picton TW. *J Clin Neurophysiol* **9** 456–479 (1992).
5. Pfefferbaum A, Roth WT and Ford JM. *Arch Gen Psychiatry* **52**, 559 (1995).
6. Nunez PL. *Electrical Fields of the Brain: The Neurophysics of EEG*. Oxford: Oxford University Press, 1981.
7. Yingling CD and Hosobuchi Y. *Electroencephalogr Clin Neurophysiol* **59**, 72–76 (1984).
8. Smith ME, Halgren E, Sokolik M et al. *Electroencephalogr Clin Neurophysiol* **76**, 235–248 (1990).
9. Halgren E, Baudena P, Clarke JM et al. *Electroencephalogr Clin Neurophysiol* **94**, 191–220 (1995).
10. Baudena P, Halgren E, Heit G et al. *Electroencephalogr Clin Neurophysiol* **94**, 251–264 (1995).

11. Knight RT, Scabini D, Woods DL *et al.* *Brain Res* **502**, 109–116 (1989).
12. Posner MI. Attention in the cognitive neurosciences. In Gazzaniga M, ed. *The Cognitive Neurosciences*. Cambridge, MA: MIT Press, 1994: 615–624.
13. Bandettini PA, Jesmanowicz A, Wong E *et al.* *Magn Reson Med* **30**, 161–173 (1993).
14. Menon V, Link KO, Anderson JH *et al.* *Behav Res Methods Comp Instr* in press.
15. Moseley ME and Glover GH. *Neuroimaging Clin N Am* **5**, 161–191 (1995).
16. Friston KJ, Williams SRT, Howard R *et al.* *Magn Reson Med* **35**, 346–355 (1996).
17. Friston KJ, Ashburner J, Poline JB *et al.* *Hum Brain Mapp* **2**, 165–189 (1995).
18. Ford I. *J Cerebr Blood Flow Metab* **15**, 371–177 (1995).
19. Friston KJ, Holmes AP, Worsley KJ *et al.* *Hum Brain Mapp* **1**, 214–220 (1994).
20. Worsley KJ and Friston KJ. *Neuroimage* **2**, 173–181 (1995).
21. Friston KJ, Worsley KJ, Frackowiak RSJ *et al.* *Hum Brain Mapp* **1**, 214–220 (1994).
22. Friston KJ, Jezzard and Turner R. *Hum Brain Mapp* **1**, 153–171 (1994).
23. Ary JP, Klein SA and Fender DH. *IEEE Trans Biomed Eng* **28**, 447–452 (1981).
24. Steinmetz H, Furst G and Meyer BU. *Electroencephalogr Clin Neurophysiol* **72**, 499–506 (1989).
25. Towle VL, Bolanos J, Suarez D *et al.* *Electroencephalogr Clin Neurophysiol* **86**, 1–6 (1993).
26. Lagerlund TD, Sharbrough FW, Jack CR *et al.* *Electroencephalogr Clin Neurophysiol* **86**, 7–14 (1993).
27. Vogt BA, Nimchinsky EA, Vogt LJ *et al.* *J Comp Neurol* **359**, 490, (1995).
28. Pedley TA and Traub RD. Physiological basis of the EEG. In: Daley DD and Pedley TA, eds. *Current Practice of Clinical Electroencephalography*. New York: Raven Press, 1990: 107–138.
29. Dale AM and Sereno MI. *J Cogn Neurosci* **5**, 162–176 (1993).
30. Mesulam MM. *Ann Neurol* **28**, 597–613 (1990).
31. Devinsky O, Morrell MJ and Vogt BA. *Brain* **118**, 279–306 (1995).
32. Risold PY and Swanson LW. *Science* **272**, 1484–1486 (1996).
33. Menon V, Lim KO, Ford JM *et al.* *Neuroimage* **3**, S234 (1996).
34. McCarthy G, Luby M, Gore JC *et al.* *Neuroimage* **3**, S548 (1996).
35. Buckner RL, Bandettini PA, O'Craven KM *et al.* *Proc Natl Acad Sci USA* **93**, 14878–14883 (1996).
36. Menon V, Ford JM, Lim KO *et al.* *Abstracts, Third International Conference on Functional Mapping of the Human Brain* (1997).

ACKNOWLEDGEMENTS: The authors thank M.J. Rosenbloom for editorial assistance. This research was supported by the Sinclair Fund, NIH (AA05965, MH30854, RR09784), the Norris Foundation, and the Department of Veteran Affairs.

**Received 20 June 1997;
accepted 20 July 1997**